

# Glucosamine Conjugated Gadolinium (III) Oxide Nanoparticles as a Novel Targeted Contrast Agent for Cancer Diagnosis in MRI

Morteza Zadeh T.<sup>1,2\*</sup>, Gholibegloo E.<sup>3</sup>, Riyahi Alam N.<sup>1\*</sup><sup>✉</sup>, Haghgo S.<sup>4</sup>, Musa A. E.<sup>1</sup>, Khoobi M.<sup>3</sup>

## ABSTRACT

**Background:** Glucose transporter (Glut), a cellular transmembrane receptor, has a key role in the metabolism of cell glucose and is also associated with various human carcinomas.

**Objective:** In this study, we evaluated a magnetic resonance (MR) imaging contrast agent for tumor detection based on paramagnetic gadolinium oxide ( $\text{Gd}_2\text{O}_3$ ) coated polycyclodextrin (PCD) and modified with glucose ( $\text{Gd}_2\text{O}_3@\text{PCD-Glu}$ ) for the targeting of overexpressed glucose receptors.

**Material and Methods:** In this experimental study, 3T magnetic resonance imaging (MRI) scanner was used to assess the specific interactions between Glut1-overexpressing tumor cells (MDA-MB-231) and  $\text{Gd}_2\text{O}_3@\text{PCD-Glu}$  NPs. Furthermore, the capacity of transporting  $\text{Gd}_2\text{O}_3@\text{PCD-Glu}$  NPs to tumor cells was evaluated.

**Results:** It was found that the acquired MRI  $T_1$  signal intensity of MDA-MB-231 cells that were treated with the  $\text{Gd}_2\text{O}_3@\text{PCD-Glu}$  NPs increased significantly. Based on the results obtained,  $\text{Gd}_2\text{O}_3@\text{PCD-Glu}$  NPs can be applied in targeting Glut1-overexpressing tumor cells *in vivo*, as well as an MRI-targeted tumor agent to enhance tumor diagnosis.

**Conclusion:** Results have shown that glucose-shell of magnetic nanoparticles has a key role in diagnosing cancer cells of high metabolic activity.

**Citation:** Morteza Zadeh T, Gholibegloo E, Riyahi Alam N, Haghgo S, Musa A. E, Khoobi M. Glucosamine Conjugated Gadolinium (III) Oxide Nanoparticles as a Novel Targeted Contrast Agent for Cancer Diagnosis in MRI. *J Biomed Phys Eng*. 2020;10(1):25-38.  
doi: 10.31661/jbpe.v0i0.1018.

## Keywords

Magnetic Resonance Imaging; Gadolinium; Contrast media

## Introduction

Carcinoma cells have a higher uptake of glucose compared to normal cells. This is due to their properties of hyper metabolism and relatively rapid proliferation [1]. This is also observed in tumor cell membranes, with higher glucose transporter (Glut) expression such as Glut-1. Glut-1, is found in most tumor cell lines and tumor tissues. Analogs, which have structural similarities with D-glucose, can also be transported by Glut-1 to Glut-4. The high metabolic needs of tumor cells lead to increased uptake of these analogs. The ability of hexose phosphate isomerase to transform D-glucose-6-phosphate into 1,

<sup>1</sup>PhD, Department of Medical Physics and Biomedical Engineering, Tehran University of Medical Sciences, Tehran, Iran

<sup>2</sup>PhD, Department of Medical Physics, School of Medicine, Tabriz University of Medical Science, Tabriz, Iran

<sup>3</sup>PhD, Department of Pharmaceutical Biomaterials and Medical Biomaterials Research Center (MBRC), Faculty of Pharmacy, Tehran University of Medical Sciences, Tehran, Iran

<sup>4</sup>PhD, Pharmaceutical Department, Food and Drug Laboratory Research Center, Food and Drug Organization (FDO), Ministry of Health, Tehran, Iran

\*Corresponding author:  
N. Riyahi Alam  
Department of Medical Physics and Biomedical Engineering, Tehran University of Medical Sciences, Tehran, Iran  
E-mail: riahinad@sina.tums.ac.ir

Received: 17 September 2018  
Accepted: 12 October 2018

6-diphosphate is hampered by these analogs. Therefore, this hinders further metabolism. Positron emission tomographic (PET) studies with fluorodeoxyglucose have been able to utilize Glut-1 for imaging tumor tissues [2, 3]. Several diagnostic substances which are in tandem with the aforementioned targeting vectors have been developed and applied in different imaging modalities such as PET, single photon emission computed tomography (SPECT) [4, 5], optical imaging [6, 7], as well as magnetic resonance imaging [8, 9].

A useful imaging modality for distinguishing cancerous masses from non-cancerous masses is PET. It can also be used in the evaluation and staging of recurrent diseases (for instance cancer). Furthermore, PET scans are used to assess the effectiveness of a treatment method by assessing death of tumor cells or in terms of their sugar consumption [10]. A commonly used glucose analog in PET imaging is 2-fluoro-2-deoxy-D-glucose molecule (<sup>18</sup>FDG). It has been shown to be efficient in tumor metabolic imaging; however, its clinical usage has been hindered as a result of high cost, inadequacy as well as difficulty in accessibility. Moreover, owing to the short half-life of positron emitting isotopes, PET imaging must be done within a very short period of time. The synthesis and chemical analysis of <sup>18</sup>FDG are time-consuming and difficult.

MRI is an effective molecular imaging (MI) modality due to its high spatial resolution as well as tremendous soft tissue contrast. MI techniques facilitate the quantification of molecular changes related to the development of pathologic states, leading to early diagnosis of diseases like cancer [11]. However, as a result of MRI low sensitivity, acquired images could suffer from insufficient contrast, hence limitation of clinical applications. To enhance contrast as well as diagnostic accuracy, several exogenous contrast agents (CAs) have been developed and applied in MRI [12]. Compared to conventional contrast agents, nanoparticles offer several merits that one of

them is loadability, in which the concentration of the imaging agent can be adjusted to suit the particular nanoparticle in the synthesis process. Tunability is also another merit, in which the circulation time of the agent in the blood stream or a target organ can be elongated. Lastly, nanoparticles have abilities to act as multifunctional MI agents because they have several features which can be utilized simultaneously in different imaging modalities such as MRI [13]. Amongst the different nanoparticles, gadolinium oxide ( $\text{Gd}_2\text{O}_3$ ) nanoparticle is mostly used as a result of its large specific surface area and good paramagnetic property (high spin magnetic moment,  $s=7/2$ ), hence making it suitable for magnetic resonance imaging (MRI) [14]. A study by Bridot et al. [15] have shown the suitability of organic dye-functionalized  $\text{Gd}_2\text{O}_3$  nanoparticles for both MRI and fluorescence imaging. Conversely, the introduction of a suitable polymer on the surface of MNPs is a way of overcoming some shortfalls of  $\text{Gd}_2\text{O}_3$  MNPs, including the strong dipole-dipole attraction between particles, safety and aggregation [16]. Moreover, efficient surface modification of MNPs offers protection to the magnetic core from the surrounding environment as well as inducing special physico-chemical properties. Hence, by attaching target groups, biological activities can be improved. Variations of MNPs with cyclodextrin (CD), a type of macrocyclic oligosaccharide, have been utilized in several ways due to favorable properties such as truncated cone chemical structure with an internal hydrophobic cavity, outstanding biocompatibility, non-toxicity, and biodegradability [17].

Earlier studies have been conducted towards improving the water solubility of Gd contrast agent by introducing various sugar groups into their structures [18, 19]. Further development of structures causing the use of glucose and galactose/mannose moieties have also been supported, by the latter used to improve targeting *in vivo* and can also serve as substrate for native enzyme [20].

Therefore, in present experimental study, CD and glucosamine on the surface of magnetic nanoparticles were spontaneously used and provided significant features for designing nano-contrast agents and consequently enhanced their solubility and stabilization. They also facilitate a magnetically conductible system to the target site as an alternative to  $^{18}\text{FDG}$  that has no radioactive half-life, widely available, cost effective, efficient anticancer effects, with very little side effects on normal human breast cells as well as highly precise in MRI oncology and cancer diagnosis at the initial stages. We also showed that these particles subsequently accumulate in the cytoplasm of MDA-MB-231 (Glut1 overexpressing tumor cells) examined by in vitro magnetic resonance imaging.

## Material and Methods

In this experimental study, breast cancer cell line MDA-MB-231 and mouse mammary cancer cell lines (4T1), MCF-10A (non-tumorigenic epithelial breast cell line), Dulbecco's modified Eagle's medium (DMEM) and Roswell Park Memorial Institute medium (RPMI-1640) cell culture media and DTPA, bare  $\text{Gd}_2\text{O}_3$  NPs (<100 nm),  $\beta$ -cyclodextrine (CD) 1-ethyl-3-[3-(dimethylamino)-propyl] carbodiimide (EDC), N-hydroxysuccinimide (NHS), phosphate-buffered saline (PBS; 10 mM, pH=7.4) were purchased from Pasteur Institute (Tehran, Iran), Gibco (USA), fetal bovine serum HyClone (USA) and Sigma Aldrich (St. Louis, MO), respectively. We procured Gd-DOTA (Dotarem®) from Bayer Health Care Pharmaceuticals Inc. (Montville, NJ, USA), while additional materials were from Merck KGaA (Darmstadt, Germany).

### Preparation of $\text{Gd}_2\text{O}_3$ @PCD-DG NPs

#### The synthesis of DTPA-dianhydride

The process of synthesizing DTPA-dianhydride has been previously described [21]. Briefly, 7.6 mmol of DTPA 3 g was dissolved in dimethyl sulfoxide 10 mL, acetic anhydride

20 mL, and pyridine 3 mL as a base under anhydrous conditions. In this step, the mixture was heated at 65 °C for 24 h. Afterwards, it was cooled, filtered, and washed twice in acetic anhydride and anhydrous diethyl ether. White powder was produced after drying the residue at constant weight under vacuum (52 kPa) at 40 °C. Application of DTPA-bis-Anhydride (DTPA-DA) as monomer in condensation polymerization endows the produced polyester with myriad acid and amide functional groups as selective gadolinium ions chelating agents preventing toxic gadolinium leakage.

#### Conjugation of D-glucosamine hydrochloride to $\text{Gd}_2\text{O}_3$ /PCD ( $\text{Gd}_2\text{O}_3$ /PCD-Glu)

$\text{Gd}_2\text{O}_3$  (0.3 g) was initially dispersed in anhydrous DMSO (10 mL). CD (0.1 mmol, 0.12 g) was then added to the as-prepared dispersion followed by addition of 0.5 mL of dried triethylamine (TEA). The reaction mixture was stirred at room temperature for at least 12 h under room temperature to form stable complex between hydroxyl group of CD and  $\text{Gd}_2\text{O}_3$ . Afterwards, DTPA-DA (0.78 mmol, 0.28 g) was added to the mixture and stirred for another 12h.  $\text{Gd}_2\text{O}_3$ /PCD was centrifuged (12000 rpm) and washed three times with deionized water and ethanol. Finally, white powder was obtained and dried in a desiccator.

Conjugation of D-glucosamine hydrochloride to  $\text{Gd}_2\text{O}_3$ /PCD ( $\text{Gd}_2\text{O}_3$ /PCD-Glu) was carried out using the following procedure: Briefly, to 0.7 g  $\text{Gd}_2\text{O}_3$ /PCD NPs dissolve in 10mL dried DMSO, 0.4g 1-ethyl-3-(3-dimethylaminopropyl) carbodiimide (EDC) and 0.3g N-hydroxysuccinimide (NHS) was added. The mixed solution was stirred under room temperature for at least 12 h. Afterwards, 0.45 g (2.5 mmol) of DG was added to the solution and stirred for another 12 h. The reaction mixture was then centrifuged (9000 rpm) and the precipitate was washed three times with deionized water and ethanol, and then dried.

### Characterization

The Fourier transform infrared (FTIR) spectra were obtained via a Nexus 670 model FTIR spectrophotometer (Thermo Nicolet, USA) at 400-4000 cm<sup>-1</sup> at room temperature using KBr pellets. 10 mg samples were heated from room temperature to 800 °C, at a heating rate of 10 °C/min in nitrogen. Zeta potential measurements were conducted using a ZetaPALS instrument (Brookhaven, USA). Nicomp 380 ZLS Zeta potential/Particle sizer (PSS Nicomp, USA) was used for DLS analysis. The concentration of Gd was measured using inductively coupled plasma atomic emission spectroscopy (ICP-OES 730-ES, Varian). FEI Magellan 400 microscope was used to obtain the field emission scanning electron microscopy (FESEM) images. X'Pert PRO MPDP-AAnalytical (Netherlands) X-ray diffractometer with Cu target (40 kV, 40 mA) was used to obtain the X-ray diffraction (XRD) patterns while JEM-1400 transmission electron microscope (Japan) was used to obtain the transmission electron microscopy (TEM) images. The sample suspension was dropped on a 200 mesh copper grid deposited by carbon, and dried in air. VSM measurements were done by VSM 7400 model (Lakeshore Cryotronics Inc., OH, USA). A 3 T MRI scanner (Siemens Prisma MRI Scanner using head coil) was used for all phantoms, in vitro, and in vivo MR imaging.

### Hemolysis assay

The procedures of a previously reported method were followed in evaluating the hemolytic activity of the prepared samples against human red blood cells (HRBCs) [22]. Briefly, centrifugation of fresh human blood stabilized with EDTA was carried out at 2000 rpm for 10 min to remove plasma as supernatant, while the resulting precipitate was rinsed in PBS (pH 7.4) and washed four times. Afterwards, PBS was used to dilute the RBC suspension 10 times. 200 µL of the diluted HRBCs suspension was added to 800 µL of each Gd<sub>2</sub>O<sub>3</sub>@PCD-Glu sample at different concentrations

(1.95–1000 mg mL<sup>-1</sup>) as well as positive (800 µL Triton X100, 2% v/v) and negative (800 µL of PBS buffer, pH 7.4) controls. Incubation of these samples lasted for 2 h at room temperature with moderate shaking. Lastly, centrifugation of all samples at 10000 rpm for 2 min was done, in addition to measuring the absorbance of supernatant (hemoglobin) via UV-visible spectrophotometer at 541 nm. The following equation was used to calculate the hemolytic activity percentage of the various samples:

$$\text{Hemolysis\%} = \frac{(Abs_{\text{Sample}} - Abs_{\text{Ctrl-}})}{(Abs_{\text{Ctrl+}} - Abs_{\text{Ctrl-}})} \times 100$$

### Cell culture

The Dulbecco's modified Eagle's medium (DMEM) supplemented with 10% of fetal bovine serum (FBS), 100 U/ml of penicillin and 100 µg/mL of streptomycin at 37 °C in a humidified incubator with 5% of CO<sub>2</sub>, was used to incubate MCF-10A (epithelial normal breast) cells lines as well as Glut1-overexpressing MDA-MB-231 (breast carcinoma) [9]. For in-vivo experiments, mouse mammary cancer cell lines (4T1) were cultured in RPMI-1640 + FBS 10%.

### Cytotoxicity assay

MTT method was used to assess the cytotoxicity of Gd<sub>2</sub>O<sub>3</sub>@PCD-Glu in MDA-MB-231 cells. In brief, 2 × 10<sup>4</sup> cells per well were seeded in 96-well plates for 24 h at 37 °C. A culture medium was then replaced with a fresh DMEM medium of varying concentrations of NPs (0, 1.5, 3.12, 6.25, 12.5, 25, 50, 100 µgr/mL). 24 and 48 h after incubation, 10 µL of MTT in a concentration of 5 mg/mL was added to each well. This was followed by incubation of the cells for an additional 4 h at 37 °C. Lastly, ELISA reader Thermo Multiscan MK3 at 570 nm, was used to measure the reaction mixture on each of the 96-well culture plate. All experiments were conducted in triplicate. The rate of survival was calculated using the following equation:

$$\% Viability = \frac{OD_{(treat)}}{OD_{(control)}} \times 100$$

OD<sub>(treated)</sub> represents the absorbance of cells incubated by nanoparticles while OD<sub>(control)</sub> signifies absorbance of cells without nanoparticles.

### Relaxivity Measurements

The diagnostic ability of Gd<sub>2</sub>O<sub>3</sub>@PCD-Glu NPs and Dotarem (clinical MRI contrast agent as a control), was evaluated according to the protocol of phantom imaging [23, 24]. Phantom agar gels of Gd<sub>2</sub>O<sub>3</sub>@PCD-Glu NPs and Dotarem were obtained from 2.5% w/v agar solutions in PBS (0.1 M, pH 7.4) with varying concentrations (0–0.64 mM (Gd), determined by ICP-MS). The imaging parameters used for measurements of T<sub>1</sub> and T<sub>2</sub> relaxation times include external field (H) = 3 T, temperature = 22 °C, NEX = 3, slice thickness = 5 mm, flip angle of 90°, the number of signal averages of 3, field of view 128 × 128 mm<sup>2</sup>, and metric sizes 256 × 256, spacing (gap) = 1 cm, and bandwidth = 15.63. T<sub>1</sub> relaxation time for each sample was obtained by varying repetition times (TR = 50, 200, 400, 600, 800, 1100, 1300, 1500, 1800, 2000 ms) with fixed echo time at TE = 11 ms. Similarly, T<sub>2</sub> relaxation times were measured by varying echo times (TE = 10, 30, 60, 90, 130, 170, 210, 240, 270, 350 ms) and fixed TR = 3,000 ms. The signal intensities of each sample were obtained using the manual approach of drawing their regions of interest. Monoexponential curve fitting of signal intensity against time (repetition or echo times) was applied in calculating the relaxation rates (R<sub>1</sub> = 1/T<sub>1</sub> and R<sub>2</sub> = 1/T<sub>2</sub>). The values of specific relaxivity (r<sub>1</sub> and r<sub>2</sub>) were obtained by fitting the curve of 1/T<sub>1</sub> and 1/T<sub>2</sub> (s<sup>-1</sup>) against the concentration of Gd (mM) in agar gels, respectively.

### MDA-MB-231 cells magnetic resonance imaging

In order to evaluate the targeting ability of

Gd<sub>2</sub>O<sub>3</sub>@PCD-Glu NPs in in-vitro, MDA-MB-231 cells (of density = 1 × 10<sup>6</sup> cells/well) were seeded into 6-well plates with 2 ml fresh medium. It was incubated afterwards at 37°C and 5% CO<sub>2</sub> overnight to achieve cell confluence. This was later substituted with a fresh non-glucose medium (2 mL) with PBS (control), Gd<sub>2</sub>O<sub>3</sub>@PCD-Glu with Gd<sup>+3</sup> concentrations of 0, 12.5, and 50 µg/mL. Cells were incubated at 37°C and 5% CO<sub>2</sub> for a further 6 h. The choice of Gd<sup>+3</sup> concentrations was according to the acceptable cytotoxicity of the MTT assay. Then, the cells were washed with PBS 5 times, trypsinized, centrifuged, and resuspended in 1 ml PBS (containing 0.5% agarose) in 2 ml Eppendorf tubes for MR imaging. A 3 T Siemens Prisma system was used for all MR imaging. Conventional spin-echo sequence with the following inputs: TR/TE = 500/12 ms, 220 × 320 matrices, 82 × 120 mm field of view, 140 Hz/Px of bandwidth, and slice thickness of 3 mm was used for the acquisition of T<sub>1</sub>-weighted images [11].

### In vivo MRI tumor imaging studies

The conduct of all animal studies was in accordance with relevant national and international guidelines of Tehran University of Medical Sciences (Approval number: IR.TUMS.REC.1394.1461). Ten female BALB/c mice (6–8 weeks old, 20–25 g) were purchased from Iran Pasteur Institute. They were housed under constant 12-h dark and light cycles, in addition to standard diet and water ad libitum. All animals were randomly assigned to two groups (5 in each): the experimental and control groups. Each animal was xenografted in the right foreleg muscle with 2 × 10<sup>6</sup> (4T1). Two weeks after grafting, the tumors had reached a size of about 1-2 cm in diameter.

The T<sub>1</sub>-contrast ability of Gd<sub>2</sub>O<sub>3</sub>@PCD-Glu NPs for targeted imaging of an in vivo tumor model was verified using mouse mammary cancer cell lines (4T1), collected via incubation with 0.05% trypsin-EDTA. They were centrifuged and resuspended in 0.2 mL PBS.

Afterwards,  $2 \times 10^6$  cells were subcutaneously implanted into the right flank of each mouse. Two weeks later, the diameter of the xeno-grafted tumor ranged between 1.0-2.0 cm. A 3 T Siemens Prisma system was also used for In vivo MR imaging. A 250  $\mu\text{L}$  of the  $\text{Gd}_2\text{O}_3@\text{PCD-Glu}$  NPs suspension was administered to mice through tail vein injection at a dose of 0.1 mg/kg Gd of body weight [25]. Dotarem was used in the control group. The  $T_1$ -weighted MR images were acquired before and 30 min, 1 h and 6 h after administration using a conventional spin-echo sequence with the following parameters: TR: 600 ms; TE: 8.6 ms; FA: 150°; slice thickness: 2 mm; FOV: 110 mm; matrix size:  $192 \times 154$  and NEX: 6.

For quantitative data analysis of  $T_1$ -weighted images, the serial post-injection MRI images were processed into DICOM (digital imaging and communication in medicine) images using Dicom Works Software (v 1.3.5) [26, 27]. The contrast-to-noise ratio (CNR) at different

time points was obtained by manually placing the region of interest (ROI) around the tumor.

### Statistical analysis

All data were presented as mean  $\pm$  standard error of the mean (SEM), while star mark was used to denote statistical significance ( $p < 0.05$ ) between groups as determined by two-tailed T-test assuming unequal variances when comparing two groups, unless particularly outlined. Significant differences ( $p < 0.05$ ) between multiple groups were determined using ANOVA.

## Results

### FTIR analysis

The FTIR spectra of DTPA-DA,  $\text{Gd}_2\text{O}_3$ ,  $\text{Gd}_2\text{O}_3@\text{PCD}$ , and  $\text{Gd}_2\text{O}_3@\text{PCD-Glu}$  are shown in Figure 1. The FTIR spectrum of  $\text{Gd}_2\text{O}_3$  core (Figure 1) shows peaks around  $1492 \text{ cm}^{-1}$ ,  $1393 \text{ cm}^{-1}$  and  $540 \text{ cm}^{-1}$  which are

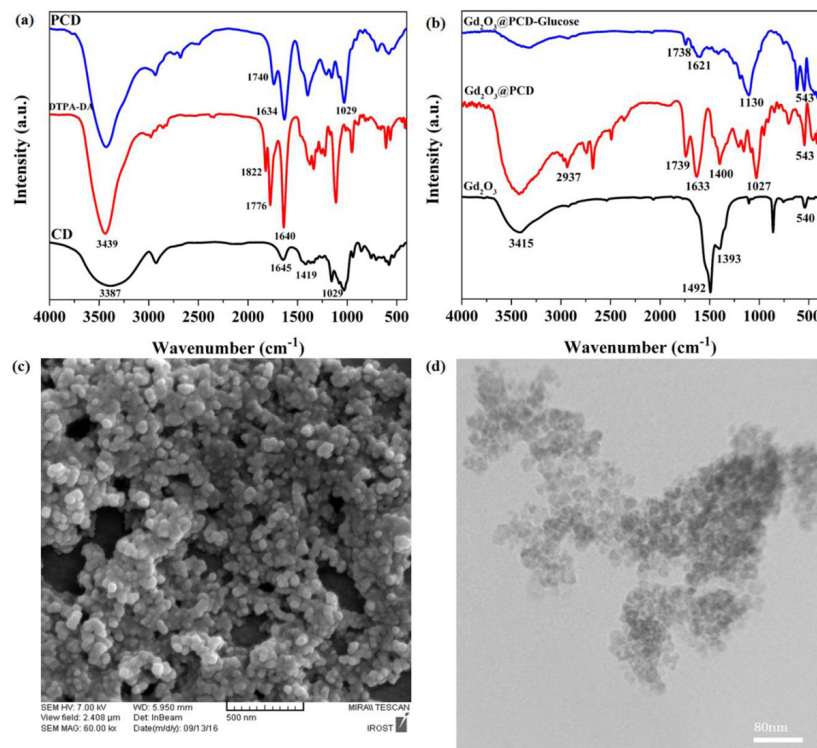


**Figure 1:** FTIR spectra of (a) CD, DTPA-DA and PCD. (b)  $\text{Gd}_2\text{O}_3$ ,  $\text{Gd}_2\text{O}_3@\text{PCD}$  and  $\text{Gd}_2\text{O}_3@\text{PCD-Glu}$  NPs. (c) FE-SEM and (d) TEM image of  $\text{Gd}_2\text{O}_3@\text{PCD-Glu}$  NPs.

related to the  $\text{Gd}=\text{O}$ ,  $\text{Gd}-\text{O}-\text{Gd}$  and  $\text{Gd}-\text{O}$  vibrations, respectively. The FTIR spectrum of DTPA-DA shows the bands at around 1822, 1776 and  $1113\text{ cm}^{-1}$  which are attributed to the asymmetric and symmetric stretching vibrations of  $\text{C}=\text{O}$  and  $\text{C}-\text{N}$  stretching in anhydride [28] (Figure 1a). The bands of  $\text{C}=\text{O}$  stretching vibrations ( $1739\text{ cm}^{-1}$  and  $1634\text{ cm}^{-1}$ ), in FTIR spectrum of  $\text{Gd}_2\text{O}_3 @\text{PCD}$  and attributed to ester and carboxylate groups, confirmed the presence of PCD moieties on the surface of the core  $\text{Gd}_2\text{O}_3$  [29] (Figure 1b).

For  $\text{Gd}_2\text{O}_3 @\text{PCD-Glu}$  (Figure 1b), the FTIR spectrum showed that the characteristic peaks of  $\text{Gd}_2\text{O}_3$  and the polymer layer have been preserved. The appeared band at around  $1130\text{ cm}^{-1}$  indicated an attachment of Glucosamine to the surface of  $\text{Gd}_2\text{O}_3 @\text{PCD}$ .

### Morphological analysis of NPs

Morphology and size assessment of the prepared samples were evaluated using FE-SEM and TEM analysis. As shown in Figures 1(a) and (b),  $\text{Gd}_2\text{O}_3 @\text{PCD-Glu}$  NPs are spherical in shape and seemed to be uniform, which is in good agreement with the results of DLS analysis. Slight differences between data from FE-SEM and DLS could be as a result of the various processes involved in preparing the samples [30].

### Dynamic light scattering (DLS) and Zeta potential analysis

DLS analysis was used to obtain the hydrodynamic size as well as size distribution of the prepared samples. Mean diameter of  $\text{Gd}_2\text{O}_3$  and  $\text{Gd}_2\text{O}_3 @\text{PCD-Glu}$  NPs was  $91 \pm 5.3$  nm (PDI= 0.321) and  $118 \pm 6.2$  nm (PDI= 0.277), respectively (Table 1). The particle size of the

prepared polymer was useful in passive tumor target delivery of drugs loaded in NPs as a result of enhanced permeability and retention effect (EPR) [31], in addition to decreasing reticuloendothelial system (RES)-mediated clearance and avoiding renal filtration [32]. Polydispersity index (PDI) < 0.5 gave an indication of the suitable size distribution of NPs. Evaluation of the surface charge of the prepared NPs was carried out by measuring the surface zeta potential. Zeta potential values of  $\text{Gd}_2\text{O}_3$  and  $\text{Gd}_2\text{O}_3 @\text{PCD-Glu}$  shifted from +23.1mV to -5.06mv due to surface modification of  $\text{Gd}_2\text{O}_3$  with cyclodextrin moieties as well as hydroxyl and carboxyl groups of the polymer coating layer.

### VSM analysis

The magnetic properties of  $\text{Gd}_2\text{O}_3$  and  $\text{Gd}_2\text{O}_3$ NPs were evaluated using a vibrating sample magnetometer (VSM) at RT (300 K) (Figure 2). The amounts of magnetic saturation values ( $\sigma_s$ ) of  $\text{Gd}_2\text{O}_3$  and  $\text{Gd}_2\text{O}_3 @\text{PCD-Glu}$  were 1 and 0.56 emu/g, respectively, hence indicating the paramagnetic property of the synthesized nanoparticles (linear relationship between magnetization (M) and applied field (H) with positive slope) [33]. The reasonable decrease in magnetization values of modified NPs can be attributed to the application of non-magnetic organic moieties (PCD) on the surface of the  $\text{Gd}_2\text{O}_3$  [34].

### Hemolysis assay

Strict hemolysis could result in serious problems. Hence, hemolysis assay was done for  $\text{Gd}_2\text{O}_3$  and  $\text{Gd}_2\text{O}_3 @\text{PCD-Glu}$  NPs in order to evaluate their biosafety and toxic effects on erythrocytes [22]. Figure 2(c) shows the he-

**Table 1:** DLS size, PDI and zeta potential of the  $\text{Gd}_2\text{O}_3$  and  $\text{Gd}_2\text{O}_3 @\text{PCD-FA-DOX}$  NPs.

Nanoparticle	Hydrodynamic diameter(nm)	PDI	Zeta potential(mv)
$\text{Gd}_2\text{O}_3$	$91 \pm 5.3$	0.321	+23.1
$\text{Gd}_2\text{O}_3 @\text{PCD-Glu}$	$118 \pm 6.2$	0.277	-5.06

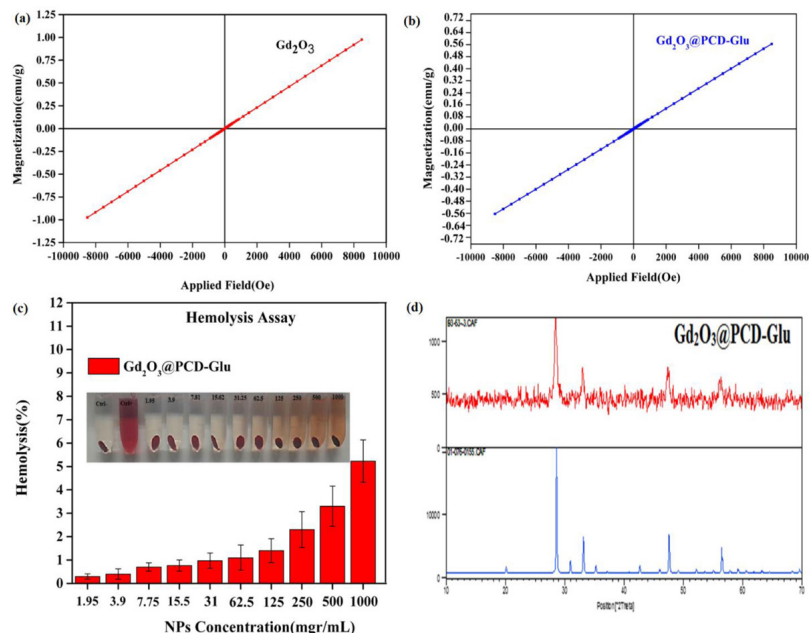


**Figure 2:** Magnetization curves of (a)  $\text{Gd}_2\text{O}_3$  (b)  $\text{Gd}_2\text{O}_3@\text{PCD-Glu}$ . Magnetization (emu/g) plotted as a function of the applied field. (c): Hemolytic activity of  $\text{Gd}_2\text{O}_3@\text{PCD-Glu}$  NPs at concentration range of 1.95–1000 mg/mL (right to left). (d) XRD pattern of the  $\text{Gd}_2\text{O}_3@\text{PCD-Glu}$  NPs.

mocompatibility of  $\text{Gd}_2\text{O}_3@\text{PCD-Glu}$  NPs similar to the negative control (PBS), which resulted in sedimentation. Whereas, hemolysis activities with no sedimentation were observed for the HRBCs treated with Triton X100 (2% v/v) (positive control). In addition, hemolytic activity of  $\text{Gd}_2\text{O}_3@\text{PCD-Glu}$  in the studied concentration range (1.95–1000 mg/mL) was less than the standard acceptance limit of 5%.

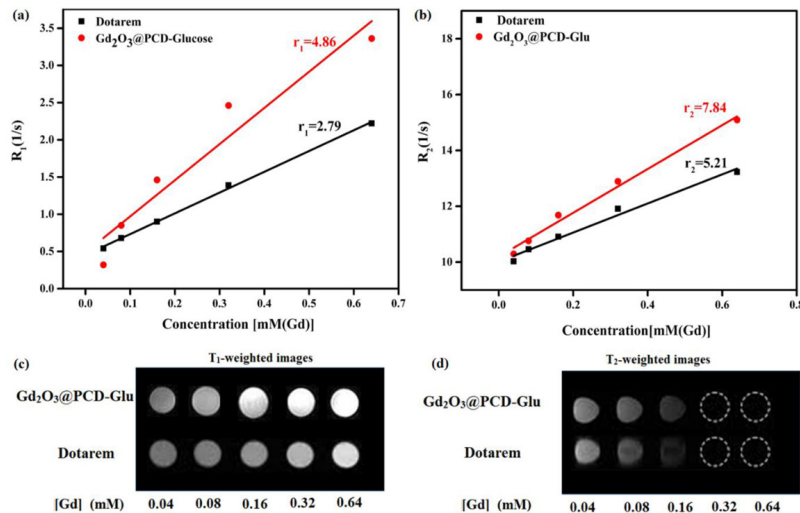
### XRD analysis

Figure 2(d) shows the XRD patterns of  $\text{Gd}_2\text{O}_3$  and  $\text{Gd}_2\text{O}_3@\text{PCD-Glu}$  NPs. The observed characteristic peaks of  $\text{Gd}_2\text{O}_3$  was in consonance with that of a previous study [35]. It also showed that the crystalline structure of  $\text{Gd}_2\text{O}_3$  was maintained after polymerization and glucoseamine conjugation processes.

### Relaxivity measurement

To evaluate the potential application of  $\text{Gd}_2\text{O}_3@\text{PCD-Glu}$  NPs as a new contrast agent,  $T_1$ - $T_2$ -weighted MRI images were performed in aqueous suspensions of the NPs at

certain concentrations. In Figure 3,  $\text{Gd}_2\text{O}_3@\text{PCD-Glu}$  showed more efficient contrast enhancement than that of Dotarem at the same concentration. The molecular structure of PCD as a coating agent is a reason for this rise in magnetic resonance sensitivity of  $\text{Gd}_2\text{O}_3@\text{PCD-Glu}$ . PCD is composed of several hydroxyl groups. As a result, it attracts water molecules, increases local water density, and also improves the rate of water exchange of  $\text{Gd}_2\text{O}_3@\text{PCD-Glu}$  [36, 37]. These in vitro MR imaging results implied that  $\text{Gd}_2\text{O}_3@\text{PCD-Glu}$  would produce same imaging effects with commercial contrast agent, Dotarem, by decreasing its dose. Gd-based complexes always are limited by adverse effects such as nephrogenic systemic fibrosis. However, a decrease in the agent's dose improves its clinical safety [38]. Quantitative analysis was done by measuring the values of the longitudinal relaxation time ( $T_1$ ) for different concentrations of Gd complex in aqueous. Figure 3 shows that the increased concentration of  $\text{Gd}_2\text{O}_3@\text{PCD-Glu}$  and Dotarem led to a decrease in  $T_1$  and an



**Figure 3:** (a)  $T_1$  and (b)  $T_2$  relaxivity plot of aqueous suspension of  $\text{Gd}_2\text{O}_3@\text{PCD-Glu}$  NPs and Dotarem. (c)  $T_1$ -weighted and (d)  $T_2$ -weighted MR images of  $\text{Gd}_2\text{O}_3@\text{PCD-Glu}$  at 3.0 T MR system.

increase in longitudinal relaxation rate  $R_1$  ( $R_1 = 1/T_1$ ). At the same time,  $\text{Gd}_2\text{O}_3@\text{PCD-Glu}$  demonstrated a shorter  $T_1$  values than Dotarem at the same concentration. Longitudinal ( $r_1$ ) and transverse ( $r_2$ ) relaxivities of the particles were calculated by measuring the relaxation rate as a function of Gd ions concentration. Calculated  $r_1$  value for  $\text{Gd}_2\text{O}_3@\text{PCD-Glu}$  was  $4.86 \text{ mM}^{-1} \cdot \text{s}^{-1}$  which was more than that of Dotarem ( $2.79 \text{ mM}^{-1} \cdot \text{s}^{-1}$ ).

#### In vitro cytotoxicity assay

Cytotoxicity of the target sample against MCF-10A epithelial normal breast and cancerous breast carcinoma MDA-MB-231 cells at treatment times of 24 and 48 h was carried out using MTT assay. As illustrated in Figure 4(a), cytotoxicity of  $\text{Gd}_2\text{O}_3@\text{PCD-Glu}$  against MCF-10A cells, as compared to control was about 7% after 24 h ( $p > 0.05$ ) and 13% after 48 h ( $p < 0.05$ ) at concentration of  $100 \mu\text{g}/\text{mL}$ , revealing their biocompatible property. It could be proposed that  $\text{Gd}_2\text{O}_3$  coating with PCD led to a reduction in Gd leakage. For MDA-MB-231 cells (Figure 4(b)), cytotoxicity of  $\text{Gd}_2\text{O}_3@\text{PCD-Glu}$  NPs, in comparison with control, was about 10% after 24 h ( $p < 0.05$ ) and 21% after 48 h ( $p < 0.05$ ) at con-

centration of  $100 \mu\text{g}/\text{mL}$ .

#### In vitro MR imaging

The use of  $\text{Gd}_2\text{O}_3@\text{PCD-Glu}$  as the probe for the *in vitro* MR imaging of MDA-MB-231 cells was evaluated. Dotarem was also investigated similarly for comparison. Figure 4(c) and (d) shows  $T_1$ -weighted MR images of MDA-MB-231 cells before and after treatment with  $\text{Gd}_2\text{O}_3@\text{PCD-Glu}$  or Dotarem for 6 h. For the MDA-MB-231 cells treated with  $\text{Gd}_2\text{O}_3@\text{PCD-Glu}$ , the *in vitro* MR signal intensities (Figure 4c) were found to have a significant increase when compared to untreated control cells or the cells treated with Dotarem. In contrast, Dotarem had no effects in the MR signal intensity.

#### In vivo MR imaging

Further investigation was conducted using  $\text{Gd}_2\text{O}_3@\text{PCD-Glu}$  as the probe for *in vivo* MR imaging of 4T1 tumors in comparison to Dotarem for similar objective. Significant visualization of tumors was observed for both  $\text{Gd}_2\text{O}_3@\text{PCD-Glu}$  and Dotarem, following intravenous injection of an aqueous suspension of  $\text{Gd}_2\text{O}_3@\text{PCD-Glu}$  or Dotarem in PBS into tumor-bearing mice. Axial  $T_1$ -

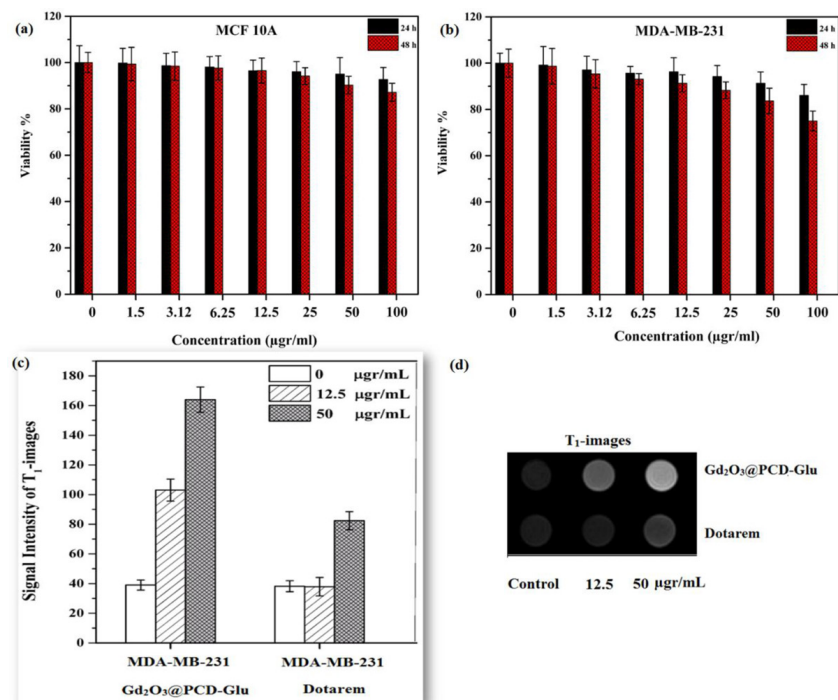


**Figure 4:** Cytotoxicity of  $\text{Gd}_2\text{O}_3@\text{PCD-Glu}$  nanoparticles measured by MTT assay in MCF 10A (a) and MDA-MB-231 (b) cells after 24 and 48 h incubation. Data is expressed as mean  $\pm$  S.E.M. ( $n = 3$ ). (c) Signal intensity analysis for  $T_1$ -weighted MR images. (d)  $T_1$ - weighted MR images of  $\text{Gd}_2\text{O}_3@\text{PCD-Glu}$  and Dotarem in MDA-MB-231 cells at different concentration of NPs after incubation for 6 h on 3T MR system.

weighted images of the tumor enhanced by the  $\text{Gd}_2\text{O}_3@\text{PCD-Glu}$  or Dotarem are shown in Figure 5. As illustrated in Figure 5, the CNR of tumor for  $\text{Gd}_2\text{O}_3@\text{PCD-Glu}$  increased from  $0.89 \pm 0.23$  to  $4.85 \pm 1.01$  within 1 h after injection and gradually reduced to  $1.99 \pm 0.36$  within 6 h. There was a steady rise in the CNR of tumor with time, up to a peak value after 1 h. Afterwards, a steady decline in the CNR was observed, and attained baseline after 6 h ( $p = 0.64$ ). In contrast, in the control group, CNR for the mice under the same treatment does not increase obviously over time post-injection and achieved  $1.22 \pm 0.23$ , 1 h after injection and reduced to  $0.95 \pm 0.22$  after 6 h (Figure 5c, P-value  $<0.05$ ).

## Discussion

In present study, the choice of DTPA as monomer for preparing cyclodextrin-based

polymer as a coating agent was due to its availability, low cost, simple polymerization method as well as proper affinity towards  $\text{Gd}^{+3}$  ions. Polymerization was accomplished between  $\beta$ -CD and DTPA-DA in the presence of naked  $\text{Gd}_2\text{O}_3$  NPs resulting in CD-based polyester containing appropriate functional groups for chelating of  $\text{Gd}_2\text{O}_3$  core as well as further functionalization. Glucoseamine was then conjugated to the appeared acidic groups on the surface of  $\text{Gd}_2\text{O}_3$  NPs to enhance the contrast agent's targeting ability. In addition, the inductively-coupled plasma atomic emission spectroscopy (ICP-AES) results showed that the Gd concentration on the final NPs was approximately 60%. Generally, it is believed that owing to the strong chelating ability of DTPA towards  $\text{Gd}^{+3}$  ions [39], DTPA was selected as monomer to prepare cyclodextrin-based polymer as a coating agent.

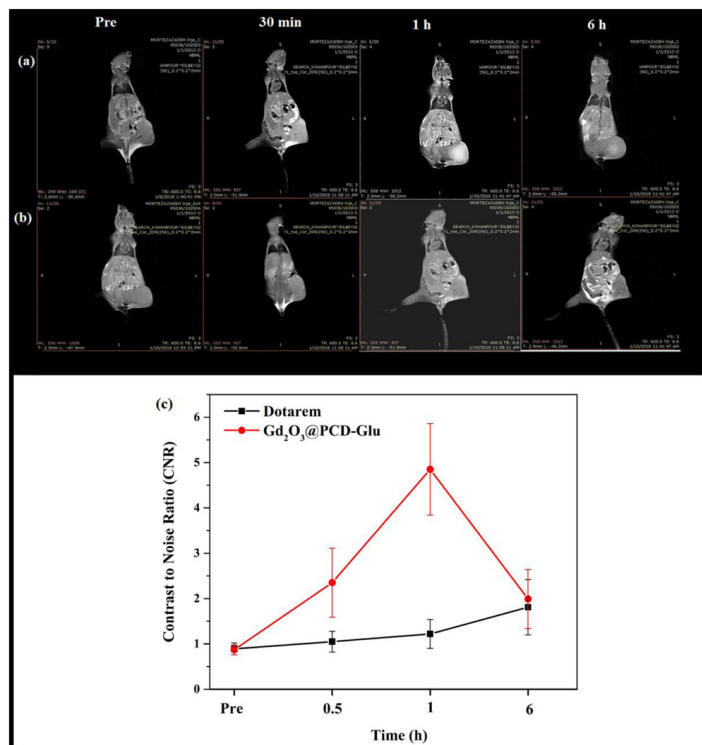


**Figure 5:** T<sub>1</sub>-weighted images of Mice tumor injected with (a) Gd<sub>2</sub>O<sub>3</sub>@PCD-Glu NPs and (b) Dotarem. (c) CNR analysis for T<sub>1</sub>-weighted images in tumor. Data represent mean  $\pm$  SEM ( $n = 5$ ), P-value < 0.05.

It has been shown by studies that negatively charged NPs have poor propensities to absorb plasma proteins. Furthermore, their stability in blood circulation is better compared to positively charged NPs. This is because adsorption of protein leads to rapid clearance of NPs from blood circulation by microphages [40, 41]. Also, negatively charged surfaces are considerably less hemolytic compared to positively charged surfaces [42].

Cytotoxicity results showed that Gd<sub>2</sub>O<sub>3</sub>@PCD-Glu NPs had less cytotoxicity against MCF-10A normal breast cells with respect to cancerous MDA-MB-231 cells due to higher metabolic rate and reproduction of cancerous cells compared to normal cells. In other words, attachment of Glucosamine to Gd<sub>2</sub>O<sub>3</sub>@PCD increased cellular uptake of Gd<sub>2</sub>O<sub>3</sub>@PCD-Glu through phospholipid cell membrane. This could probably be due to the overexpression of Glut-1 receptors over the MDA-MB-231

cell surface, leading to more accumulation in the cytoplasm [9]. Increased uptake of these analogs was a result of the increased metabolic needs of the tumor cells.

Relaxivity measurements exhibited that introduction of PCD could be led to an increase in the molecular weight of contrast agent, extension of rotation time and consequently increased the relaxivity. According to literature, polar C=O groups in the polymer coating layer endow the contrast agent with acceptable water accessibility [43]. In some cases, poor water accessibility to the intraparticular Gd<sup>3+</sup> ions inside the polymer can compromise the performance of T<sub>1</sub>-weighted MRI [44]. This challenge can be tackled using porous materials through which a water molecule can travel from the bulk water into the interior space [45, 46]. Proper relaxivity of Gd<sub>2</sub>O<sub>3</sub>@PCD-Glu in our study after coating with PCD as a hydrophilic polymer layer could be due to the pres-

ence of polar carbonyl groups on the surface of  $\text{Gd}_2\text{O}_3$  core. Water molecules easily diffused across this porous membrane.

Based on *in vitro* MRI results, our design facilitates significant targeting uptake of the particles in MDA-MB-231 cells overexpressing Glut1. *In vivo* MR imaging results indicate that  $\text{Gd}_2\text{O}_3@\text{PCD-Glu}$  could clearly and selectively enhance the contrast at the tumor area in  $T_1$ -weighted MR images which could be due to targeting ability of NPs because of over-expression of Glut-1 receptors over the cell surface. Cancer cells require more glucose compared to normal cells due to their hyper metabolism and high rate of proliferation [47].  $\text{Gd}_2\text{O}_3@\text{PCD-Glu}$ , having structural similarities with D-glucose, can be transported by Glut-1 to Glut-4. An increase in the uptake of these analogs due to increased metabolic needs of tumor cells is observed during this period. Ethylenedicycysteine-deoxyglucose (EC-DG), a glucose derivative, was developed by Yang et al. [48]. Their findings showed that it is involved in growth as well as proliferation of cells. Due to the similarities in the pathway(s) of glucosamine and glucose, it facilitates post-treatment follow-ups.

## Conclusion

In summary, a new gadolinium (III)-based complex  $\text{Gd}_2\text{O}_3@\text{PCD-Glu}$  as a novel nano-contrast agent was successfully synthesized for MR molecular imaging. They have proper paramagnetic property, cyto-compatibility, blood-compatibility and high magnetic relaxivity for MR imaging and were suitable for intravenous injection. In terms of  $r_1$  and  $T_1$ -weighted *in vitro* imaging,  $\text{Gd}_2\text{O}_3@\text{PCD-Glu}$  gave a better relaxation performance compared to commercial Dotarem. Hence,  $\text{Gd}_2\text{O}_3@\text{PCD-Glu}$  could serve as an efficient probe for targeted MR imaging *in vitro* as well as xenografted animal model tumors *in vivo*. The use of  $\text{Gd}_2\text{O}_3@\text{PCD-Glu}$  could allow for early detection of primary tumors as well as tumor metastasis. It also shows great promise

in monitoring the reappearance of tumors.

## Acknowledgment

This work was supported in part by the Research Chancellor of Tehran University of Medical Sciences (Grant no. 94-03-30-30035) Tehran, Iran.

## Conflict of Interest

None

## References

- Farhood B, Raei B, Ameri H, Shirvani M, Alizadeh A, Najafi M, et al. A review of incidence and mortality of colorectal, lung, liver, thyroid and bladder cancers in Iran and compared to other countries. *Contemp Oncol.* 2019;23(1):7. doi: 10.5114/wo.2019.84112. PubMed PMID: 31061631.
- Clavo AC, Brown RS, Wahl RL. Fluorodeoxyglucose uptake in human cancer cell lines is increased by hypoxia. *J Nucl Med.* 1995;36:1625-32. PubMed PMID: 7658223.
- Haberkorn U, Ziegler SI, Oberdorfer F, Trojan H, Haag D, Peschke P, et al. FDG uptake, tumor proliferation and expression of glycolysis associated genes in animal tumor models. *Nucl Med Biol.* 1994;21:827-34. doi: 10.1016/0969-8051(94)90162-7. PubMed PMID: 9234332.
- Yang DJ, Kim CG, Schechter NR, Azhdarinia A, Yu DF, Oh CS, et al. Imaging with 99mTc ECDG targeted at the multifunctional glucose transport system: feasibility study with rodents. *Radiology.* 2003;226:465-73. doi: 10.1148/radiol.2262011811. PubMed PMID: 12563141.
- Chen Y, Huang ZW, He L, Zheng SL, Li JL, Qin DL. Synthesis and evaluation of a technetium-99m-labeled diethylenetriaminepentaacetate-deoxyglucose complex ([99mTc]-DTPA-DG) as a potential imaging modality for tumors. *Appl Radiat Isot.* 2006;64:342-7. doi: 10.1016/j.apradiso.2005.08.004. PubMed PMID: 16290170.
- Zhang W, Chen Y, Guo DJ, Huang ZW, Cai L, He L. The synthesis of a D-glucosamine contrast agent, Gd-DTPA-DG, and its application in cancer molecular imaging with MRI. *Eur J Radiol.* 2011;79:369-74. doi: 10.1016/j.ejrad.2010.10.021. PubMed PMID: 21106316.
- Cheng Z, Levi J, Xiong Z, Gheysens O, Keren S, Chen X, et al. Near-infrared fluorescent deoxyglucose analogue for tumor optical imaging in cell culture and living mice. *Bioconjug Chem.* 2006;17:662-9. doi: 10.1021/bc050345c. PubMed PMID: 16704203. PubMed PMCID: PMC3191878.
- Kovar JL, Volcheck W, Sevick-Muraca E, Simpson MA, Olive DM. Characterization and performance of a near-infrared 2-deoxyglucose optical imaging agent for mouse cancer models. *Anal Biochem.* 2009;384:254-62. doi:

- 10.1016/j.ab.2008.09.050. PubMed PMID: 18938129. PubMed PMCID: PMC2720560.
9. Shan XH, Hu H, Xiong F, Gu N, Geng XD, Zhu W, et al. Targeting Glut1-overexpressing MDA-MB-231 cells with 2-deoxy-d-glucose modified SPIOs. *Eur J Radiol*. 2012;81:95-9. doi: 10.1016/j.ejrad.2011.03.013.
10. Cheze-Le Rest C, Metges JP, Teyton P, Jestin-Le Taillec V, Lozac'h P, Volant A, et al. Prognostic value of initial fluorodeoxyglucose-PET in esophageal cancer: a prospective study. *Nucl Med Commun*. 2008;29:628-35. doi: 10.1097/MNM.0b013e328f81423. PubMed PMID: 18528185.
11. Mortezaee T, Gholibegloo E, Alam NR, Dehghani S, Haghgo S, Ghanaati H, et al. Gadolinium (III) oxide nanoparticles coated with folic acid-functionalized poly ( $\beta$ -cyclodextrin-co-pentetic acid) as a biocompatible targeted nano-contrast agent for cancer diagnostic: in vitro and in vivo studies. *MAGMA*. 2019;32(4):487-500. doi: 10.1007/s10334-019-00738-2. PubMed PMID: 30730021.
12. Dehghani S, Alam NR, Shahriarian S, Mortezaee T, Haghgo S, Golmohamadpour A, et al. The effect of size and aspect ratio of Fe-MIL-88B-NH<sub>2</sub> metal-organic frameworks on their relaxivity and contrast enhancement properties in MRI: in vitro and in vivo studies. *J Nanoparticle Res*. 2018;20(10):278. doi: 10.1007/s11051-018-4376-2.
13. Gholibegloo E, Mortezaee T, Salehian F, Forootanfar H, Firoozpour L, Foroumadi A, et al. Folic acid decorated magnetic nanospunge: An efficient nanosystem for targeted curcumin delivery and magnetic resonance imaging. *Journal of Colloid and Interface Science*. 2019;556:128-39. doi:10.1016/j.jcis.2019.08.046.
14. Narmani A, Farhood B, Hagh-Aminjan H, Mortezaee T, Aliasgharzadeh A, Mohseni M, et al. Gadolinium nanoparticles as diagnostic and therapeutic agents: Their delivery systems in magnetic resonance imaging and neutron capture therapy. *J Drug Deliv Sci Technol*. 2018;44:457-66. doi: 10.1016/j.jddst.2018.01.011.
15. Bridot JL, Faure AC, Laurent S, Riviere C, Billotey C, Hiba B, et al. Hybrid gadolinium oxide nanoparticles: multimodal contrast agents for in vivo imaging. *J Am Chem Soc*. 2007;129:5076-84. doi: 10.1021/ja068356j. PubMed PMID: 17397154.
16. Chen X, Zhu J, Chen Z, Xu C, Wang Y, Yao C. A novel bienzyme glucose biosensor based on three-layer Au-Fe3O4@SiO<sub>2</sub> magnetic nanocomposite. *Sensors and Actuators B: Chemical*. 2011;159:220-8. doi: 10.1016/j.snb.2011.06.076.
17. Gholibegloo E, Mortezaee T, Salehian F, Ramazani A, Amanlou M, Khoobi M. Improved curcumin loading, release, solubility and toxicity by tuning the molar ratio of cross-linker to  $\beta$ -cyclodextrin. *Carbohydr Polym*. 2019;213:70-8. doi: 10.1016/j.jddst.2018.01.011.
18. Fulton DA, Elemento EM, Aime S, Chaabane L, Botta M, Parker D. Glycoconjugates of gadolinium complexes for MRI applications. *Chem Commun (Camb)*. 2006:1064-6. doi: 10.1039/b517997a. PubMed PMID: 16514440.
19. Parker D, Dickins RS, Puschmann H, Crossland C, Howard JA. Being excited by lanthanide coordination complexes: aqua species, chirality, excited-state chemistry, and exchange dynamics. *Chem Rev*. 2002;102:1977-2010. doi: 10.1021/cr010452+. PubMed PMID: 12059260.
20. Alauddin MM, Louie AY, Shahinian A, Meade TJ, Conti PS. Receptor mediated uptake of a radiolabeled contrast agent sensitive to beta-galactosidase activity. *Nucl Med Biol*. 2003;30:261-5. PubMed PMID: 12745017.
21. Duarte MG, Gil MH, Peters JA, Colet JM, Elst LV, Muller RN, et al. Synthesis, characterization, and relaxivity of two linear Gd(DTPA)-polymer conjugates. *Bioconjug Chem*. 2001;12:170-7. doi: 10.1021/bc000065r. PubMed PMID: 11312677.
22. Li J, Zheng L, Cai H, Sun W, Shen M, Zhang G, et al. Polyethyleneimine-mediated synthesis of folic acid-targeted iron oxide nanoparticles for in vivo tumor MR imaging. *Biomaterials*. 2013;34:8382-92. doi: 10.1016/j.biomaterials.2013.07.070. PubMed PMID: 23932250.
23. Daryasari MP, Akhgar MR, Mamashli F, Bigdeli B, Khoobi M. Chitosan-folate coated mesoporous silica nanoparticles as a smart and pH-sensitive system for curcumin delivery. *Rsc Advances*. 2016;6:105578-88. doi: 10.1039/c6ra23182a.
24. Zhang P, Hu L, Yin Q, Zhang Z, Feng L, Li Y. Transferrin-conjugated polyphosphoester hybrid micelle loading paclitaxel for brain-targeting delivery: synthesis, preparation and in vivo evaluation. *J Control Release*. 2012;159:429-34. doi: 10.1016/j.jconrel.2012.01.031. PubMed PMID: 22306333.
25. Azizian G, Riyahi-Alam N, Haghgo S, Moghimi HR, Zohdiaghdam R, Rafiei B, et al. Synthesis route and three different core-shell impacts on magnetic characterization of gadolinium oxide-based nanoparticles as new contrast agents for molecular magnetic resonance imaging. *Nanoscale Res Lett*. 2012;7:549. doi: 10.1186/1556-276X-7-549. PubMed PMID: 23033866. PubMed PMCID: PMC3499173.
26. Ahmad MW, Xu W, Kim SJ, Baeck JS, Chang Y, Bae JE, et al. Potential dual imaging nanoparticle: Gd203 nanoparticle. *Sci Rep*. 2015;5:8549. doi: 10.1038/srep08549. PubMed PMID: 25707374. PubMed PMCID: PMC4338476.
27. Van Vlerken LE, Amiji MM. Multi-functional polymeric nanoparticles for tumour-targeted drug delivery. *Expert Opin Drug Deliv*. 2006;3:205-16. doi: 10.1517/17425247.3.2.205. PubMed PMID: 16506948.
28. Puech PA, Boussel L, Belfkih S, Lemaitre L, Douek P, Beuscart R. DicomWorks: software for reviewing DICOM studies and promoting low-cost teleradiology. *J Digit Imaging*. 2007;20:122-30. doi: 10.1007/s10278-007-

- 9018-7. PubMed PMID: 17333414. PubMed PMCID: PMC3043902.
29. Kalender W. Classic papers in modern diagnostic radiology. Springer Science & Business Media; 2004.
  30. Ardestani MS, Arabzadeh AJ, Heidari Z, Hosseinzadeh A, Ebrahimi H, Hashemi E, et al. Novel and facile methods for the synthesis of DTPA-mono-amide: a new completely revised strategy in radiopharmaceutical chemistry. *Journal of radioanalytical and nuclear chemistry*. 2010;283:447-55.
  31. Heydarnezhadi S, Alam NR, Haghgoo S, Ghanaati H, Khoobi M, Gorji E, et al. Glycosylated Gadolinium as Potential Metabolic Contrast Agent vs Gd-DTPA for Metabolism of Tumor Tissue in Magnetic Resonance Imaging. *Applied Magnetic Resonance*. 2016;47:375-85. doi: 10.1007/s00723-015-0756-2.
  32. Gao Z, Lukyanov AN, Singhal A, Torchilin VP. Diacyl lipid-polymer micelles as nanocarriers for poorly soluble anticancer drugs. *Nano letters*. 2002;2:979-82. doi: 10.1021/nl025604a.
  33. Duan X, Li Y. Physicochemical characteristics of nanoparticles affect circulation, biodistribution, cellular internalization, and trafficking. *Small*. 2013;9:1521-32. doi: 10.1002/smll.201201390. PubMed PMID: 23019091.
  34. Honary S, Zahir F. Effect of zeta potential on the properties of nano-drug delivery systems-a review (Part 2). *Tropical Journal of Pharmaceutical Research*. 2013;12:265-73. doi: 10.4314/tjpr.v12i2.20.
  35. Sarmento B, Mazzaglia D, Bonferoni MC, Neto AP, Do Céu Monteiro M, Seabra V. Effect of chitosan coating in overcoming the phagocytosis of insulin loaded solid lipid nanoparticles by mononuclear phagocyte system. *Carbohydrate polymers*. 2011;84:919-25. doi: 10.1016/j.carbpol.2010.12.042.
  36. Akrami M, Khoobi M, Khalilvand-Sedagheh M, Haririan I, Bahador A, Faramarzi MA, et al. Evaluation of multilayer coated magnetic nanoparticles as biocompatible curcumin delivery platforms for breast cancer treatment. *RSC Advances*. 2015;5:88096-107. doi: 10.1039/c5ra13838h.
  37. Kumar S, Meena VK, Hazari PP, Sharma RK. FITC-Dextran entrapped and silica coated gadolinium oxide nanoparticles for synchronous optical and magnetic resonance imaging applications. *Int J Pharm*. 2016;506:242-52. doi: 10.1016/j.ijpharm.2016.03.040. PubMed PMID: 27032564.
  38. Tarasi R, Khoobi M, Niknejad H, Ramazani A, Ma'mani L, Bahadorikhahili S, et al.  $\beta$ -cyclodextrin functionalized poly (5-amidoisophthalicacid) grafted Fe 3 O 4 magnetic nanoparticles: A novel biocompatible nanocomposite for targeted docetaxel delivery. *Journal of Magnetism and Magnetic Materials*. 2016;417:451-9. doi: 10.1016/j.jmmm.2016.05.080.
  39. Liu Y, Yang P, Wang W, Dong H, Lin J. Fabrication and photoluminescence properties of hollow Gd 2 O 3 : Ln (Ln= Eu3+, Sm3+) spheres via a sacrificial template method. *CrystEngComm*. 2010;12:3717-23. doi: 10.1039/c0ce00145g.
  40. Dobrovolskaia MA, Aggarwal P, Hall JB, McNeil SE. Pre-clinical studies to understand nanoparticle interaction with the immune system and its potential effects on nanoparticle biodistribution. *Mol Pharm*. 2008;5:487-95. doi: 10.1021/mp800032f. PubMed PMID: 18510338. PubMed PMCID: PMC2613572.
  41. Yim H, Yang SG, Jeon YS, Park IS, Kim M, Lee DH, et al. The performance of gadolinium diethylene triamine pentaacetate-pullulan hepatocyte-specific T1 contrast agent for MRI. *Biomaterials*. 2011;32:5187-94. doi: 10.1016/j.biomaterials.2011.03.069. PubMed PMID: 21561660.
  42. Werner EJ, Datta A, Jocher CJ, Raymond KN. High-relaxivity MRI contrast agents: where coordination chemistry meets medical imaging. *Angew Chem Int Ed Engl*. 2008;47:8568-80. doi: 10.1002/anie.200800212. PubMed PMID: 18825758.
  43. Lew S, Brooks MV. Nephrogenic systemic fibrosis: clinical review and education for nurse practitioners. *The Journal for Nurse Practitioners*. 2009;5:344-9. doi: 10.1016/j.nurpra.2008.10.011.
  44. Fang J, Chandrasekharan P, Liu X-L, Yang Y, Lv Y-B, Yang C-T, et al. Manipulating the surface coating of ultra-small Gd2O3 nanoparticles for improved T1-weighted MR imaging. *Biomaterials*. 2014;35:1636-42. doi: 10.1016/j.biomaterials.2013.11.032.
  45. Chen KJ, Wolahan SM, Wang H, Hsu CH, Chang HW, Durazo A, et al. A small MRI contrast agent library of gadolinium(III)-encapsulated supramolecular nanoparticles for improved relaxivity and sensitivity. *Biomaterials*. 2011;32:2160-5. doi: 10.1016/j.biomaterials.2010.11.043. PubMed PMID: 21167594. PubMed PMCID: PMC3032383.
  46. Cheng Z, Thorek DL, Tsourkas A. Gadolinium-conjugated dendrimer nanoclusters as a tumor-targeted T1 magnetic resonance imaging contrast agent. *Angew Chem Int Ed Engl*. 2010;49:346-50. doi: 10.1002/anie.200905133. PubMed PMID: 19967688. PubMed PMCID: PMC2862691.
  47. Cheng Z, Thorek DL, Tsourkas A. Porous Polymericosomes with Encapsulated Gd-labeled Dendrimers as Highly Efficient MRI Contrast Agents. *Adv Funct Mater*. 2009;19:3753-9. doi: 10.1002/adfm.200901253. PubMed PMID: 23293575. PubMed PMCID: PMC3536029.
  48. Young CD, Lewis AS, Rudolph MC, Ruehle MD, Jackman MR, Yun JJ, et al. Modulation of glucose transporter 1 (GLUT1) expression levels alters mouse mammary tumor cell growth in vitro and in vivo. *PLoS One*. 2011;6:e23205. doi: 10.1371/journal.pone.0023205. PubMed PMID: 21826239. PubMed PMCID: PMC3149640.